Journal of
Marine Science and Engineering

Article

A Theoretical Methodology and Measurement of Dynamic Characteristics of Wind Turbines with Composite Bucket Foundations

Jijian Lian [1,2], Huan Zhou [1,2] and Xiaofeng Dong [1,2,*]

[1] State Key Laboratory of Hydraulic Engineering Simulation and Safety, Tianjin University, Tianjin 300350, China; jjlian@tju.edu.cn (J.L.); zhouhuan@tju.edu.cn (H.Z.)
[2] School of Civil Engineering, Tianjin University, Tianjin 300350, China
* Correspondence: tju_skl@126.com

Abstract: A composite bucket foundation (CBF) is a new type of supporting structure in offshore wind engineering. Its huge transition part is the key difference compared to other offshore foundations. Firstly, the vibration measurement system of a wind turbine with the CBF is introduced. A finite element method (FEM) was developed, and the rigid deformation performance of the transition part was characterized. Then, to clarify the influence of the transition part brings to wind turbines with CBFs, a three-DOF theoretical model was established by simplifying the transition part as a rigid body. Horizontal and rotational foundation stiffness were considered to present the constraint effect below the mudline. Sensitivity studies were conducted on the parameters (including mass, moment of inertia and mass center height) of the transition part. Further, the vibration properties of the CBF structures under different operation load conditions were compared through the theoretical model and the in situ data. The results show that the relative errors between the theoretical model and FEM model are 3.78% to 5.03%, satisfying the accuracy requirements. The parameters of the transition part have varying degrees of influence on the natural frequency, foundation stiffness and vibration response of the wind turbines with CBFs. Compared to wind and 1P loads, the 3P load has a greater influence if the 3P frequency is close to the natural frequency of the wind turbine.

Keywords: composite bucket foundation; transition part; theoretical model; measurement; operation load

check for updates

Citation: Lian, J.; Zhou, H.; Dong, X. A Theoretical Methodology and Measurement of Dynamic Characteristics of Wind Turbines with Composite Bucket Foundations. *J. Mar. Sci. Eng.* **2024**, *12*, 106. https://doi.org/10.3390/jmse12010106

Academic Editor: José António Correia

Received: 1 December 2023
Revised: 30 December 2023
Accepted: 3 January 2024
Published: 5 January 2024

1. Introduction

The current global energy structure still primarily relies on non-renewable fossil fuels, and the issues of the energy crisis and environmental pollution are becoming increasingly prominent. Developing renewable energy is an important way to ensure sustainable development for humanity. Wind energy is one of the most widely used and rapidly developing renewable energy sources, including onshore and offshore wind energy. Offshore wind energy has become a global focus due to its abundant reserves, minimal land use, proximity to load centers and suitability for large-scale development. According to the Global Wind Energy Council (GWEC) statistics, the global offshore market grew on average by 21% each year in the past decade, bringing total installations to 64.3 GW at the end of 2022, and GWEC Market Intelligence expects more than 380 GW of new offshore wind capacity to be added over the next decade [1].

The foundation types of offshore wind structures have shown a diversified development trend in the efficient development and utilization of offshore wind energy. Several types of offshore foundations have been applied and developed to different extents, such as the mono-pile foundation [2], multi-pile foundation [3], jacket foundation [4] and bucket foundation [5]. The bucket foundation is mainly composed of a bucket inserted into the soil and a transition part above the mudline. Compared to other foundations, it has several advantages, such as easy construction and installation, good resistance to overturning and steel material savings. In recent years, the bucket foundations have occupied a certain market share as some designs have successfully been applied in engineering, including the mono-bucket foundation (MBF) [6], bucket jacket foundation (BJF) [7] and composite bucket foundation (CBF) [8], as shown in Figure 1. The MBF consists of a single suction bucket and a single steel column transition part. The BJF is composed of the suction bucket(s) and jacket-type transition part. The CBF is proposed by China's Tianjin University. It consists of a single suction bucket and a curved reinforced concrete transition part, making it suitable for the widely distributed weak coastal soils in China.

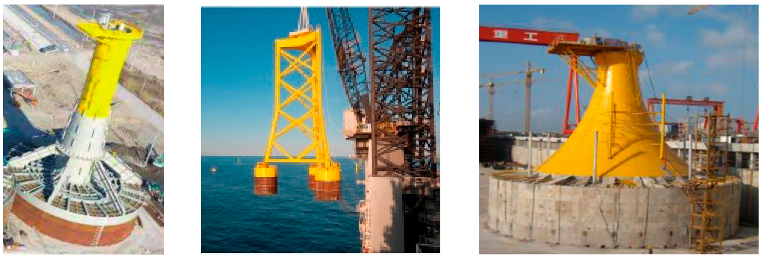

(**a**) (**b**) (**c**)

Figure 1. Bucket foundation applications: (**a**) MBF; (**b**) BJF; (**c**) CBF.

Studying the dynamic characteristics of the bucket foundation structure is of great significance for its design and the operation safety of wind turbines. Houlsby et al. [9,10] conducted model tests of the MBF and tetrapod foundation under cyclic load conditions and observed the variation in the foundation stiffness. Nielsen SD et al. [11] studied the behavior of an MBF in situ after a half year of measurement. In [12], Wang B et al. compared the dynamic performance of a monopile and an MBF in conjunction with the geological conditions of the East China Sea; it is recommended to use bucket foundations in the deep sea. Zhang PY et al. [13] conducted shaking table tests for the MBF and CBF and compared their responses under seismic load conditions. The results show that CBFs are safer than MBFs during earthquakes. Yu TS et al. [14,15] studied the dynamic response characteristics of the CBF, considering the combination of wave and current loads. Liu GW et al. [16] conducted a three-dimensional numerical simulation to calculate the wave forces on the CBF and suggest the selection of the Morison equation or diffraction theory using the relative diameter of the CBF. Ding HY et al. [17,18] carried out extensive tests on three- and four-bucket BJFs and compared their dynamic performance under seismic load conditions; the results prove the inhibition effects of the three-bucket BJFs on the seismic responses of soils. Jalbi et al. [19] developed analytical solutions to predict the natural frequencies of the BJF wind turbines, which may impact the choice of foundations for jackets.

It is clear that many studies have been conducted on the dynamic characteristics of the bucket foundations, but there is still a lack of studies in some respects. On the one hand, the studies are based on the whole bucket foundation structure, there are few studies focusing on the transition part and there is a lack of suitable model to describe the CBF and its transition part. On the other hand, the dynamic analyses in the tests and numerical simulations are mainly conducted under seismic, wind and wave load conditions, and there are few studies focusing on operation loads. Hence, the main scope of this work was to study the dynamic characteristics of the CBF transition part at a theoretical level and to compare the vibration properties of different operation loads. For calculation convenience, the transition part should be simplified, and the finite element method (FEM) is necessary to demonstrate the simplification. To build a rational FEM model of the CBF structure, a practical CBF structure is needed. Therefore, this paper mainly consists of four parts. Firstly, Section 2 introduces the main information of a CBF wind turbine and the structural vibration monitoring system. The FEM was used to study the deformation of the CBF transition part, as outlined in Section 3. The establishment and verification of the theoretical model of the CBF structure is presented in Section 4. Thirdly, Section 5 contains the detailed analyses of the influence of the transition part parameters (mass, moment of inertia and mass center height) on the CBF structure (natural frequency, foundation stiffness and vibration properties). Finally, the vibration performance of the operation loads (1P/3P/wind load) is compared in Section 6.

2. In Situ Measurement of a Composite Bucket Foundation Structure

2.1. Structure and Measurement System

The study site is a wind farm in Xiangshui, Jiangsu, China. Its center is about 10 km offshore, and the water depth is from 8 m to 12 m [20], as shown in Figure 2a. The farm has a total capacity of 202 MW, consisting of 55 wind turbines. The world's first commercially applied CBF was installed in this wind farm to support a 3.0 MW turbine, as shown in Figure 2b. The CBF was towed from factory to the installation location for 112 h and 290 nautical miles, and the installation work took 8 h, with a horizontal accuracy of 0.03%. The main parameters of the whole CBF structure are listed in Table 1.

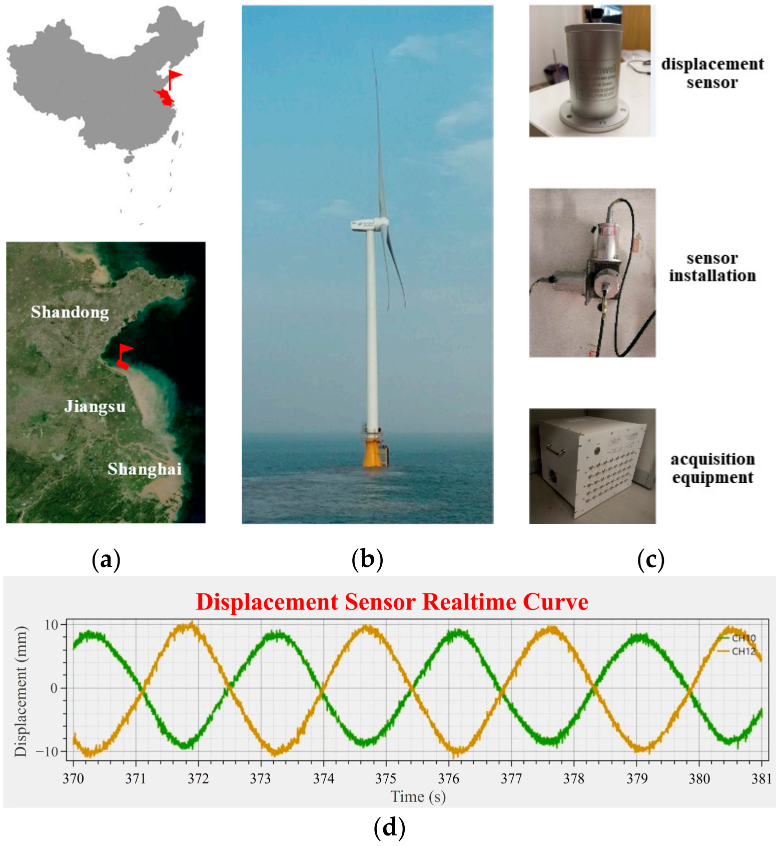

Figure 2. Information of the CBF structure: (**a**) Xiangshui wind farm location; (**b**) the CBF structure; (**c**) vibration displacement sensor and acquisition equipment; (**d**) displacement sensor real-time curve.

Table 1. Main parameters of the CBF structure.

	Parameter	Value		Parameter	Value
Turbine	head mass (t)	190	Suction bucket	height (m)	10
	rotation frequency range (RPM [1])	7.5~13.5		diameter (m)	30
Tower	mass (t)	207	Transition part	mass (t)	1949
	height (m)	73.59		height (m)	23
	diameter (m)	3.2~4.3		mass center height (m)	5.5
	thickness (mm)	14~48		thickness (mm)	600
				diameter (m)	4.3~20.6

[1] RPM = revolutions per minute.

To determine the vibration properties of the structure, a monitoring system was equipped in the wind turbine. Low-frequency vibration displacement sensors have been installed at the tower top to obtain its dynamic movement with the lowest frequency of 0.1 Hz [21], and acquisition equipment is located at the entrance platform with the sampling frequency of 300 Hz, as shown in Figure 2c. Figure 2d shows the sensors' real-time curve of measured displacement.

Based on the modal analysis method SSI (stochastic subspace identification) [22], Table 2 lists the first three orders of natural frequency results of the in situ measurement of the CBF structure. Detailed analysis of the displacement may be found in [21].

Table 2. The first three orders of natural frequency results of the in situ measurement of the CBF structure.

First Order (Hz)	Second Order (Hz)	Third Order (Hz)
0.350	2.501	5.010

2.2. Operation and Environmental Measurement

The structure has been tested in situ for a long period after installation. During vibration testing, operation and environmental information (such as wind speed, rotation speed, power and pitch angle) were also recorded simultaneously by the supervisory control and data acquisition (SCADA) system of the wind turbine. Figure 3 shows the history of wind and rotation speed and their relationship from 2 November 2017 to 8 November 2017. The value of a single point is the mean value of every 100 s. The wind speed range during the test period is from 0 to 15.57 m·s^{-1}, and the rotation speed changes from 0 to 13.5 RPM, including all turbine working conditions from park to rated generation. From Figure 3c, the operation strategy is clear: With the increase in wind speed, the wind turbine changes from park condition to generation state, the cut-in rotation speed is 7.5 RPM. Then, when the wind speed grows from 4.5 m·s^{-1} to 8 m·s^{-1}, the rotation speed grows until it reaches the rated rotation speed of 13.5 RPM. Subsequently, the rotor works stably at the rated speed, though wind speed may continually grow.

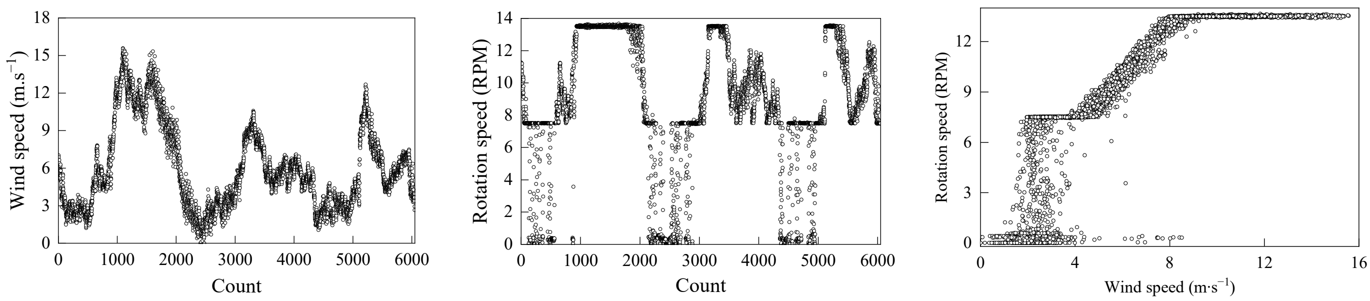

(**a**) (**b**) (**c**)

Figure 3. The history of wind and rotation speed and their relationship: (**a**) wind history; (**b**) rotation speed history; (**c**) relationship between wind and rotation speed.

3. Finite Element Modeling

Taking the above mentioned CBF structure as the research object, an ABAQUS model was established using the finite element method, as shown in Figure 4a. The head of the wind turbine was simplified as a mass point placed at the top of the tower. The tower material is Q345E steel, and the transition part is prestressed concrete structure, with C60 concrete and Q235 steel. The steel materials have a density of 7850 kg·m^{-3}, elastic modulus of 206 GPa and Poisson's ratio of 0.3, and the concrete has a density of 2500 kg·m^{-3}, elastic modulus of 36 GPa and Poisson's ratio of 0.25. Rayleigh damping was used for structural damping, with a damping ratio of 2%. An elastic constitutive model was adopted for the whole CBF structure, and the soil was simulated using the Mohr–Coulomb constitutive model. A tie connection was adopted between the tower and foundation, while surface-to-surface contact was used to simulate the interaction between the CBF and soil. Hard contact was applied in the normal direction, and the friction coefficient was set to 0.3 in the tangent direction [23]. The tower and CBF were simulated using 3D shell elements (S4R); the transition part and soil were simulated using 3D solid elements (C3D8), and the grid meshing was performed using the sweep technique. In order to ensure the computational efficiency and numerical accuracy, the local area involved in contact interaction of the model was refined, and mesh density sensitivity analysis was performed. The total number of meshes was about 100,000, and the minimum element size was $0.005D_s$ (D_s is the diameter of the foundation skirt). To eliminate boundary effects, the radius of the soil was taken as $4D_s$, and the depth was taken as $6H_s$ (H_s is the height of the foundation skirt). The bottom boundary of the foundation was fixed, and the lateral boundary only allowed vertical displacement. The soil parameters are listed in Table 3.

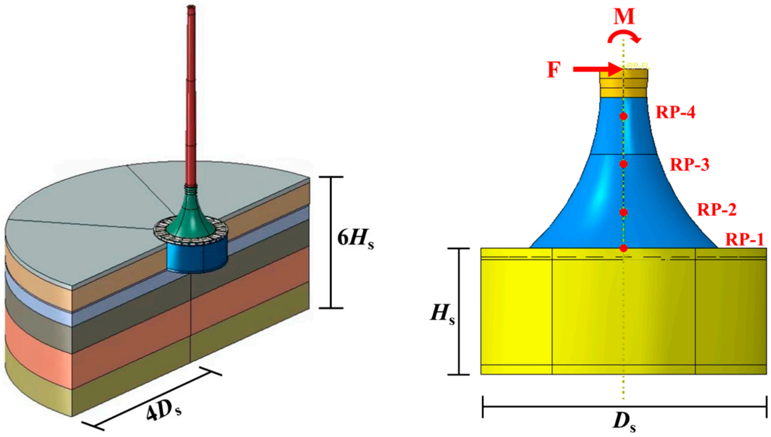

(**a**) (**b**)

Figure 4. The finite model of the CBF structure: (**a**) whole structure; (**b**) CBF model.

Table 3. The soil parameters of the CBF structure.

Layer	Soil Type	Thickness (m)	Submerged Unit Weight (kN·m^{-3})	Compression Modulus (MPa)	Friction Angle (°)	Cohesion (kPa)
1	Sandy clay	2.1	9.7	4.0	33.8	5.0
2	Silty clay	9.5	8.7	4.8	11.9	22.0
3	Silt	6.6	8.9	6.4	29.3	8.4
4	Sandy clay	11.6	8.7	6.4	12.7	23.9
5	Silt	15.4	8.9	6.4	29.3	8.4
6	Fine sand	11.8	8.7	12.6	12.0	25.0

At the equivalent points on the top of the transition part, horizontal forces and bending moments were applied in the horizontal and rotational directions, respectively, as shown in Figure 4b. The displacements of four reference points (RPs) were observed. The four RPs are key nodes of the transition part, and the heights are 1.20 m, 7.34 m, 11.98 m and 17.00 m from the mudline, respectively, as shown in Figure 4b.

The displacements at four RPs under horizontal force conditions of 50 kN, 100 kN, 250 kN, 500 kN and 1000 kN are shown in Figure 5a. It can be observed that the displacements at different points under the same force conditions are linearly related. There is no relative distortion between the top and bottom of the transition part, indicating that the CBF transition part has linear deformation under horizontal force conditions.

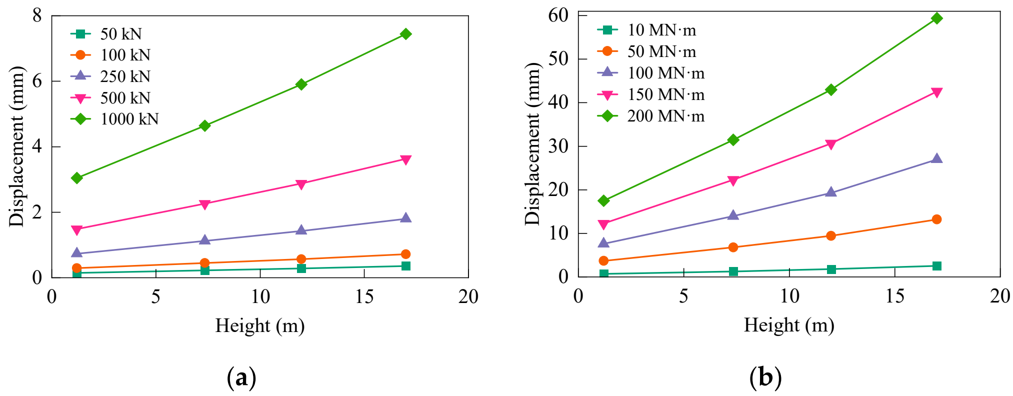

Figure 5. The deformation of the CBF transition part: (**a**) under horizontal force conditions; (**b**) under bending moment conditions.

When applying bending moments, with values of 10 MN·m, 50 MN·m, 100 MN·m, 150 MN·m and 200 MN·m, the displacements at four RPs are shown in Figure 5b. Similarly, when the bending moment does not exceed 100 MN·m, the displacements at the four RPs still show a linear relationship. Only when the moment reaches 150 MN·m does turning occur in the line, but the trend is not significant. So, it can still be approximately considered that the CBF transition part has linear deformation under bending moment conditions.

Therefore, the transition part of the CBF can be simplified as a rigid body and transformed into a mass point with mass m_f and moment of inertia I_f placed at the mass center height.

4. Establishing the Dynamic Model of the CBF Structure

The load of a practical wind structure is complicated; the FEM has a complex modeling process and a time-consuming calculation process, so neither method is suitable for structural dynamic analysis. To make clear how the transition part influences the CBF structure, it is better to establish a theoretical model so that the factors can be quantitatively analyzed one-by-one.

4.1. Motion Equation

The theoretical model of the CBF structure was established in the xz plane, as shown in Figure 6. The head of the wind turbine (including impeller, hub and nacelle, etc.) was simplified to a centralized mass point m with a rigid connection to the tower, ignoring the mass overhang. The tower was simplified to an elastic beam, with length h and bending stiffness k_t. Based on the analysis in Section 3, the transition part (height H) is regarded as a mass point, with mass m_f and moment of inertia I_f. The distance from the mass point to the mud surface is the mass center height h_f. The constraint effect of the CBF below the mudline to the wind turbine is equivalent to the horizontal stiffness k_L and rotational stiffness k_R.

As can be seen, the theoretical model vibrates in the xz plane and has three degrees of freedom (DOFs), q_1 represents the tower-top relative deformation with respect to the foundation and q_2 and q_3 donate the horizontal displacement and rotation angle of the foundation, respectively.

The Lagrange motion Equation (1) is used to derive the motion equation of the CBF structure [24]:

$$\frac{\mathrm{d}}{\mathrm{d}t}\left(\frac{\partial T}{\partial q_k'}\right) - \frac{\partial T}{\partial q_k} + \frac{\partial V}{\partial q_k} + \frac{\partial D}{\partial q_k'} = F_k,\ k = 1,\ 2,\ \cdots,\ n \tag{1}$$

where T is the kinetic energy of the entire vibration system; V is the potential energy of the entire vibration system; D is the system energy dissipation function, which is defined as the work carried out by the damping force of the system during the vibration process; q_k (k = 1, 2, $\cdots$, n) are generalized coordinates; F_k is the generalized force corresponding to the k-th generalized coordinate; and n is the number of DOFs of the system, n is 3 for this model.

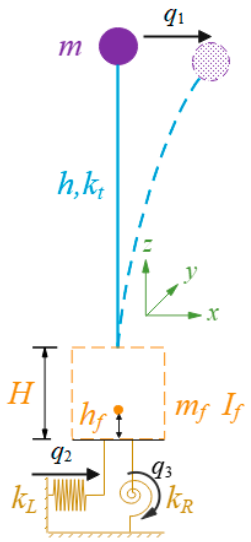

Figure 6. The theoretical model of a CBF structure.

From Figure 6, the absolute displacement of the head (u_h), tower (u_t) and foundation (u_f) of the structure can be expressed as:

$$u_h = q_1 + q_2 + L\tan(q_3) \approx q_1 + q_2 + Lq_3 \tag{2}$$

$$u_t = q_1\varphi_{1t} + q_2 + z\tan(q_3) \approx q_1\varphi_{1t} + q_2 + zq_3 \tag{3}$$

$$u_f = q_1\varphi_{1t,h_f} + q_2 + h_f\tan(q_3) \approx q_1\varphi_{1t,h_f} + q_2 + h_f q_3 \tag{4}$$

where $L = h + H$, φ_{1t} is the vibration mode of the tower, and φ_{1t,h_f} refers to the value of vibration mode at the height of transition part mass center ($z = h_f$).

The total kinetic energy T of the CBF structure can be obtained with the following equation:

$$T = \frac{1}{2}mu_h'^2 + \frac{1}{2}\int_H^L \tilde{m}u_t'^2 dz + \frac{1}{2}m_f u_f'^2 + \frac{1}{2}I_f q_3'^2 \tag{5}$$

where $\tilde{m}$ is the mass per unit length of the tower.

The total potential energy V of the whole system is:

$$\begin{aligned} V &= \tfrac{1}{2}k_t q_1^2 + \tfrac{1}{2}k_L q_2^2 + \tfrac{1}{2}k_R q_3^2 \\ k_t &= \textstyle\int_H^L EI(z)(\varphi_{1t}'')^2 \mathrm{d}z \end{aligned} \tag{6}$$

where k_t is the stiffness of the tower [25].

System energy dissipation function D [26] is defined as:

$$D = \frac{1}{2}c_h u_h'^2 + \frac{1}{2}c_L q_2'^2 + \frac{1}{2}c_R q_3'^2 \tag{7}$$

where c_h is the damping at the head, and c_L and c_R refer to the horizontal and rotational damping of the foundation, respectively.

Introducing Formulas (5)–(7) into Formula (1), the motion equation of the CBF structure can be obtained as follows:

$$\boldsymbol{M}\boldsymbol{q}'' + \boldsymbol{C}\boldsymbol{q}' + \boldsymbol{K}\boldsymbol{q} = \boldsymbol{F}(t) \tag{8}$$

where

$$\boldsymbol{M}=\begin{bmatrix} m+M_{1t} & m+M_{2t} & mL+M_{3t} \\ m+M_{2t} & m+\widetilde{m}h+m_f & mL+\frac{1}{2}\widetilde{m}\left(L^2-H^2\right)+m_f h_f \\ mL+M_{3t} & mL+\frac{1}{2}\widetilde{m}\left(L^2-H^2\right)+m_f h_f & mL^2+\frac{1}{3}\widetilde{m}\left(L^3-H^3\right)+m_f {h_f}^2+I_f \end{bmatrix} \quad (9)$$

$$M_{1t}=\widetilde{m}\int_H^L \varphi_{1t}^2 dz+m_f\varphi_{1t,h_f}^2,\ M_{2t}=\widetilde{m}\int_H^L \varphi_{1t} dz+m_f\varphi_{1t,h_f},\ M_{3t}=\widetilde{m}\int_H^L \varphi_{1t} z dz+m_f h_f\varphi_{1t,h_f} \quad (10)$$

$$\boldsymbol{C}=\begin{bmatrix} c_h & 0 & 0 \\ 0 & c_L & 0 \\ 0 & 0 & c_R \end{bmatrix} \quad (11)$$

$$\boldsymbol{K}=\begin{bmatrix} k_t & 0 & 0 \\ 0 & k_L & 0 \\ 0 & 0 & k_R \end{bmatrix} \quad (12)$$

For such a low damping structure like the wind turbine structure, the coupling effect caused by the non-diagonal elements in matrix $\boldsymbol{C}$ is negligible compared with that of diagonal elements, so only the diagonal elements are retained [27]. The damping ratios in this study were all set to 2% Rayleigh damping [28].

4.2. Foundation Stiffness

A genetic algorithm (GA) is a random search algorithm that borrows from the natural selection and genetic mechanisms in the biological world. Starting from any initial population, it continuously reproduces and evolves generation-by-generation through random selection, crossover and mutation operation and finally converges to a group of individuals which is the most fitted to the environment to find the optimal solution to problems [29]. The GA has high parallel computing capabilities and good scalability and has widely used in wind engineering to optimize wind farm layout, power production and structural design [30–32]. Before solving the motion Equation (9), the foundation stiffness k_L and k_R are obtained by the GA to ensure that the natural frequency results of the CBF structure meet the requirements. The target function is defined as the sum of percentage difference between the natural frequency results and the natural frequency targets, as shown in Equation (13). The smaller the sum, the more accurate the result is. The calculation process of GA to solve the foundation stiffness is shown in Figure 7, and the GA parameters used are shown in Table 4.

$$\min\ target=\sum_{i=1}^{N}\frac{\left|f-f_{np}\right|}{f_{np}}\times 100\% \quad (13)$$

where min represents minimum of the sum; N is the order of the natural frequencies, specifically, N = 3 in this study; $\boldsymbol{f}$ is the natural frequency results simulated by the GA; and $\boldsymbol{f_{np}}$ is the natural frequency target.

4.3. Loading

Compared with other types of tall structures, operation loads are additional loads for wind turbines due to rotation of the rotor. Operation loads mainly include the fluctuating wind load, 1P load and 3P load [33]. The 1P/3P loads are derived from the 1P/3P vibration generated by the rotation of the rotor. Their load frequencies are equal to the rotor rotation frequency (1P frequency) and the blade passing frequency (3P frequency), respectively. In recent studies, there is a lack of understanding of the influence of each operation load. Therefore, this study investigated the dynamic characteristics of the CBF structure by separately considering the effects of the 1P load, 3P load and wind load.

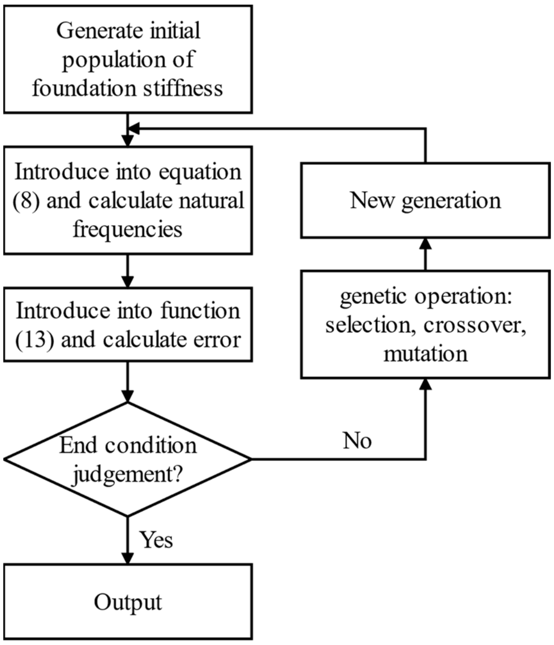

Figure 7. Flowchart of foundation stiffness calculation by the GA.

Table 4. The GA parameters for solving foundation stiffness.

Initial Population	Maximum Genetic Generation	Selection Type	Crossover Rate	Mutation Rate
300	100	roulette	0.6	0.05

In practical engineering, the 1P/3P load can be quite complex. For simplicity of calculation, sinusoidal functions were adopted in this study to simplify the 1P/3P load.

$$\begin{aligned} F_{1P} &= \sqrt{2} f_{1P} \sin(2\pi\omega t) \\ F_{3P} &= \sqrt{2} f_{3P} \sin(6\pi\omega t) \end{aligned} \quad (14)$$

where F_{1P} and F_{3P} are the 1P load and 3P load, respectively; f_{1P}, f_{3P} are the root mean square (RMS) value of the loads; and ω is the wind turbine rotation frequency.

The characteristic parameters reflecting the properties of fluctuating wind include turbulence intensity, turbulence integral length and pulsating wind speed power spectrum. The Det Norske Veritas (DNV) specification [34] recommends using the Kaimal spectrum to obtain the required wind speed, and the wind speed spectrum can be written as follows:

$$S_U(f) = \frac{4I^2 U_{10} L_k}{(1 + 6 f L_k / U_{10})^{5/3}} \quad (15)$$

where f represents the frequency, U_{10} is the average wind speed in 10 min, I is the turbulence intensity, and L_k is the turbulence integral length, which can be determined by the following formula:

$$L_k = \begin{cases} 5.67z & z < 60\ \text{m} \\ 340.2 & z \geq 60\ \text{m} \end{cases} \quad (16)$$

where z is the height above sea level.

Figure 8 shows the time history of 100 s of fluctuating wind, where the turbulence intensity is 0.1, and the sampling frequency is 100 Hz. In the actual calculation, the wind speed is multiplied by a certain coefficient to obtain the required value of wind load.

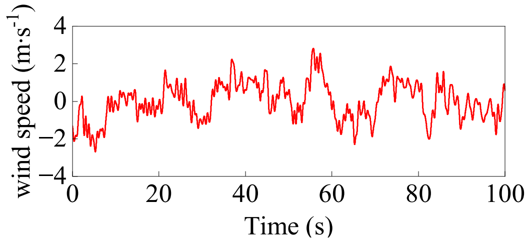

Figure 8. Time history of 100 s of fluctuating wind.

4.4. Verification of the Model

The rationality of the theoretical model was verified by comparing its dynamic response with the FEM model. To reduce the diversity of the two models, the mode shape of the theoretical model is an approximate fitting of the FEM model, considering the linear deformation properties of the transition part. In this article, only the first-order mode is considered, and the mode shape is formulated with Equation (17). It can be seen from Figure 9 that the two mode shapes are proximal, and the mode shape defied by Equation (17) is rational.

$$\begin{aligned} &\boldsymbol{c} = \{\ c_1\quad c_2\quad c_3\quad c_4\quad c_5\quad c_6\ \}^{\mathrm{T}} = \{\ -0.3114\quad -0.3755\quad 0.1777\quad 0.3902\quad 0.0652\quad 0.0004\ \}^{\mathrm{T}} \\ &\lambda_1 = 1.54922;\ \lambda_2 = 1.49869 \\ &\varphi_{1t}\left(\overline{h}\right) = \begin{cases} c_1\sin\left(\lambda_1\overline{h}\right) + c_2\cos\left(\lambda_1\overline{h}\right) + c_3\sinh\left(\lambda_2\overline{h}\right) + c_4\cosh\left(\lambda_2\overline{h}\right) & \frac{H}{L} < \overline{h} \le 1 \\ c_5\overline{h} + c_6 & 0 \le \overline{h} \le \frac{H}{L} \end{cases} \end{aligned} \tag{17}$$

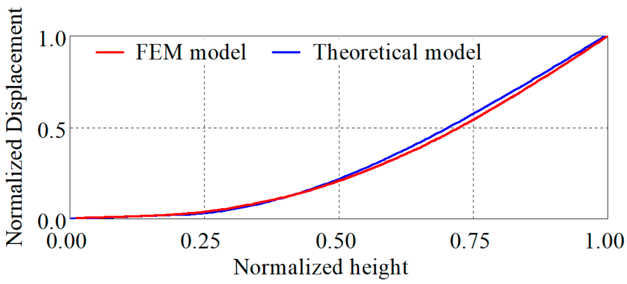

Figure 9. The mode shape of the tower.

Based on the fluctuating wind in Figure 9, the wind load of the root mean square (RMS) value 10 kN was generated and added to the tower top of the FEM model and the theoretical model, respectively. The absolute displacements of the head and foundation were extracted, as shown in Figure 10. As can be seen from the figure, the displacement time history of both models is basically the same; only the gap around 50 s is obvious. The RMS and maximum displacement values of the two models were calculated, as listed in Table 5. The head displacements of the theoretical model are 2.80 mm and 6.80 mm, and the foundation displacements of the theoretical model are 0.66 mm and 1.67 mm. The relative errors of the two models are from 3.78% to 5.03%, indicating that the theoretical model in this paper meets the accuracy requirement and is reasonable.

Table 5. The displacements and errors.

Displacement		FEM (mm)	Theoretical Model (mm)	Error (%)
Head	RMS	2.91	2.80	3.78
	maximum	7.13	6.80	4.63
Foundation	RMS	0.69	0.66	4.28
	maximum	1.76	1.67	5.03

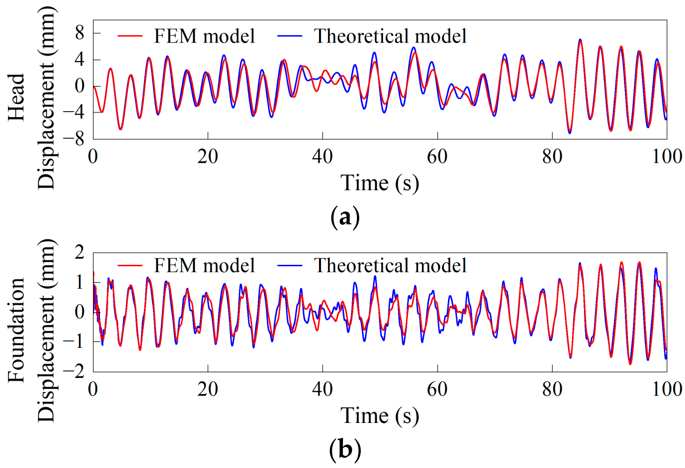

Figure 10. The displacement time history of the two models: (**a**) tower top; (**b**) foundation.

5. Analysis of the Influence of the Transition Part Parameters on the CBF Structure

First, a CBF structure model was built. The tower length was h = 75 m, the diameter was D = 4 m, the wall thickness was 30 mm and the section bending stiffness EI was 290 GPa. The head mass was set to 100 t. The height of the transition part H = 25 m, total mass $m_f = 7.34 \times 10^4$ kg, moment of initial is $I_f = 1.54 \times 10^7$ kg·m^2 and mass center height h_f = 12.5 m. The original natural frequency targets were $\boldsymbol{f}_{np}$ = [0.3 2.3 7.8] Hz, and the foundation stiffness obtained by GA was 1.92×10^7 N·m^{-1}, 3.62×10^{10} N·m·rad^{-1}. The influence of transition part parameters (m_f, I_f, h_f) was analyzed with the theoretical model based on the above values.

5.1. Influence on the Natural Frequencies of the Structure

Figure 11 shows the influence of transition part mass on the first three orders of natural frequencies of the CBF structure. The value of the right axis is the ratio of each point to the initial value. The mass ranges from 7.34×10^4 kg to 1.0×10^6 kg. It can be seen that the increase in the transition part mass causes the decrease in the natural frequencies, in which the first order shows a linear trend, and the second and third order show a gradually slowing trend. Comparing the ratios, the first and third order decrease by about 6%, but the second order decreases by 60%, indicating that the transition part mass mainly influences the second-order natural frequency.

Figure 12 shows the influence of the transition part moment of inertia on the first three orders of natural frequencies of the CBF structure. The moment of inertia ranges from 1.54×10^7 kg·m^2 to 3.0×10^7 kg·m^2. It can be seen that the increase in the moment of inertia causes the decrease in the third natural frequency by 23%, but the first- and second-order frequencies stay unchanged, indicating that the transition part moment of inertia has no effect on the first two natural frequencies; it only causes the third-order frequency reduction.

Figure 13 shows the influence of the transition part mass center height on the first three orders of natural frequencies of the CBF structure. The height ranges from 0 m (transition part bottom) to 25 m (transition part top). It can be seen that the increase in the mass center height causes the decrease in the first-order frequency by 0.7% and causes the increase in the second and third-order frequencies by about 8%, indicating that the transition part mass center height has a slight influence on the natural frequencies of the CBF structure.

5.2. Influence on the Foundation Stiffness

When the transition parameters change, the foundation stiffness provided below the CBF mudline should also be changed to meet the natural frequency design requirements of the wind turbine. In the following comparisons, the natural frequencies [0.3 2.3 7.8] Hz remain unchanged.

Figure 14 shows the influence of the transition part mass on the foundation stiffness of the CBF structure. As can be seen, the mass grows from 7.34×10^4 kg to 1.0×10^6 kg, the horizontal stiffness increases linearly by 6.97 times and the increase in rotational stiffness gradually slows down, with an increase rate of 11.14%, indicating that the transition part mass mainly affects the horizontal stiffness.

Figure 15 shows the influence of the transition part moment of inertia on the foundation stiffness of the CBF structure. As can be seen, the moment of inertia grows from 1.54×10^7 kg·m^2 to 3.0×10^7 kg·m^2, and the horizontal stiffness maximally increases by only 0.06%, while the rotational stiffness increases linearly by 96%. Therefore, it can be considered that the transition part moment of inertia mainly affects the rotational stiffness and has no effect on the horizontal stiffness.

Figure 16 shows the influence of the transition part mass center height on the foundation stiffness of the CBF structure. It can be seen that the two stiffnesses show a similar linear decrease as the mass center height rises from 0 m to 25 m. The change rate compared with the original height is about 17%, indicating that the height change in the mass center has the same influence on the two stiffnesses.

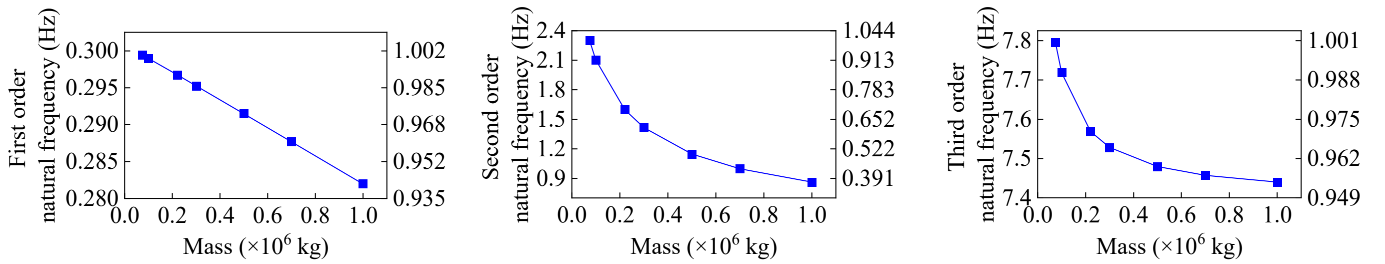

(**a**) (**b**) (**c**)

Figure 11. The influence of the transition part mass on the natural frequencies: (**a**) first order; (**b**) second order; (**c**) third order.

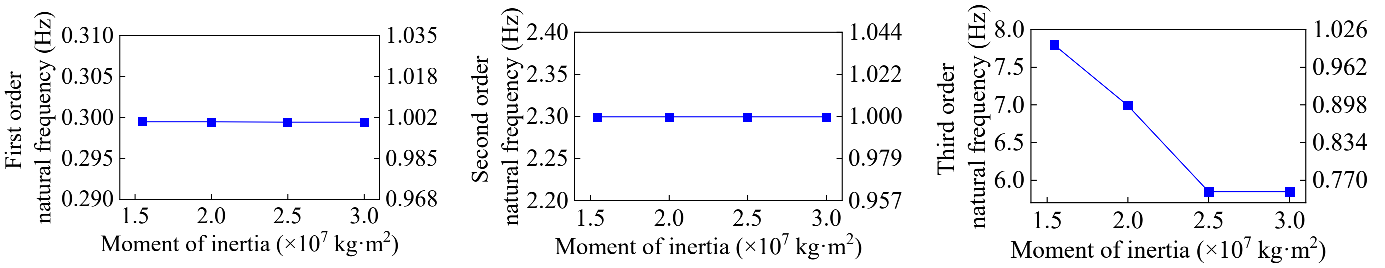

(**a**) (**b**) (**c**)

Figure 12. The influence of the transition part moment of inertia on the natural frequencies: (**a**) first order; (**b**) second order; (**c**) third order.

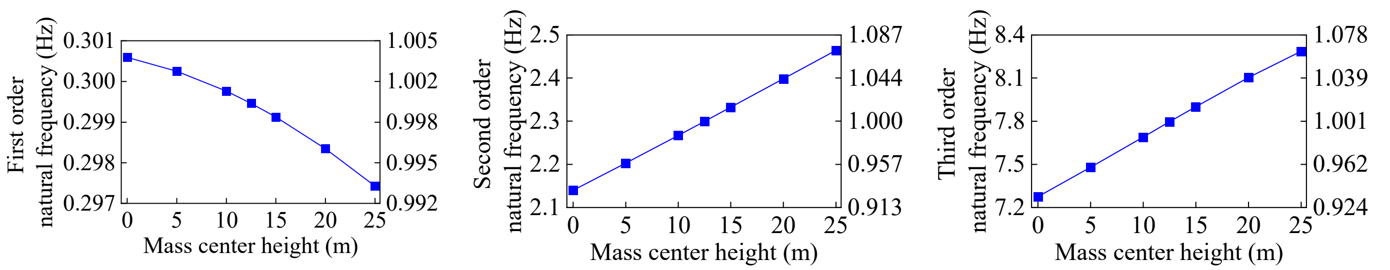

(**a**) (**b**) (**c**)

Figure 13. The influence of the transition part mass center height on the natural frequencies: (**a**) first order; (**b**) second order; (**c**) third order.

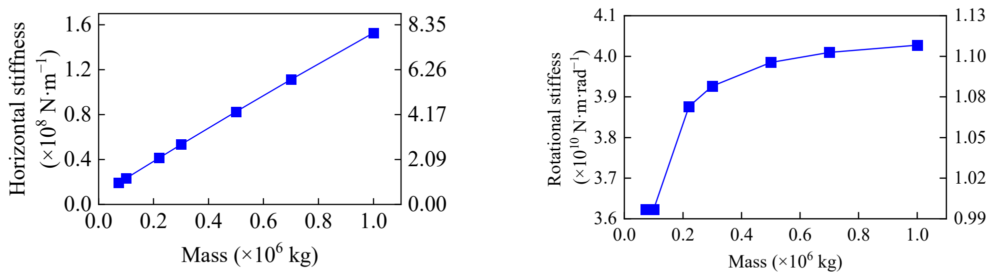

(**a**) (**b**)

Figure 14. The influence of the transition part mass on the foundation stiffness: (**a**) horizontal stiffness; (**b**) rotational stiffness.

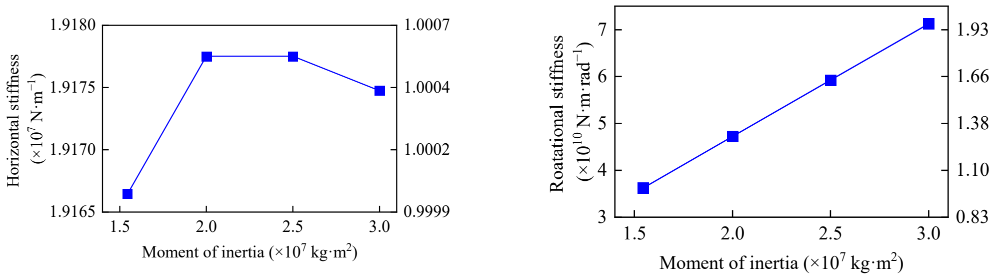

(**a**) (**b**)

Figure 15. The influence of the transition part moment of inertia on the foundation stiffness: (**a**) horizontal stiffness; (**b**) rotational stiffness.

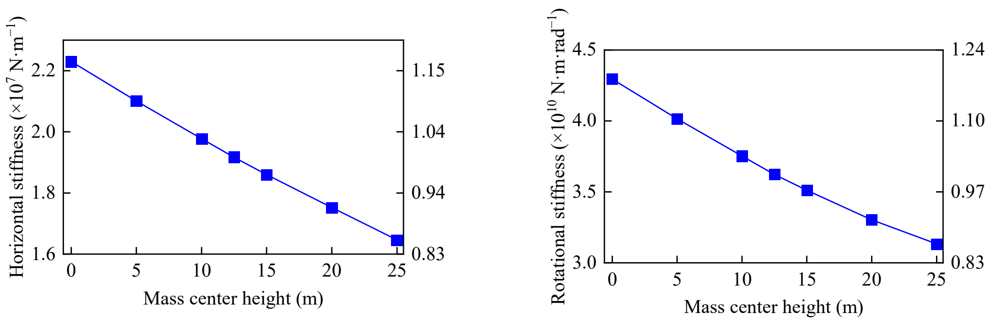

(**a**) (**b**)

Figure 16. The influence of the transition part mass center height on the foundation stiffness: (**a**) horizontal stiffness; (**b**) rotational stiffness.

5.3. Influence on the Vibration Properties

When analyzing the influence of transition part parameters on the vibration properties of the CBF structure, the input load is also the fluctuating wind load of the RMS, 10 kN, and the calculation time is 100 s. The head displacement RMS value of the wind turbine was taken to represent the vibration response. The results are shown in Figure 17.

Figure 17a is the influence of the transition part mass on the vibration properties. It can be seen that the displacement increases first and then decreases with the mass of the transition part, and the peak 3.67 mm appears at 2.20×10^5 kg. It was found that the displacement is largest when the transition part mass is equal to the tower mass; if the transition part mass is different from the tower mass, the displacement is rapidly reduced. Generally, the CBF has a huge transition part, whose mass is much greater than the tower mass. Accordingly, enlarging the transition part mass can reduce the vibration of the structure.

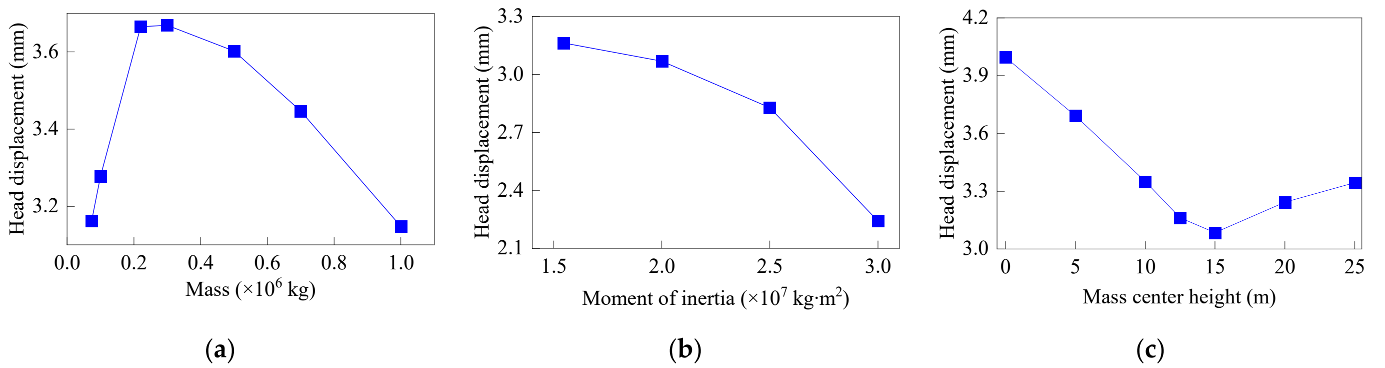

Figure 17. The influence of transition part parameters on the vibration properties: (**a**) mass; (**b**) moment of inertia; (**c**) height of mass center.

Figure 17b shows the influence of the transition part moment of inertia on the vibration properties. It can be seen that with the increase in the moment of inertia, the displacement gradually decreases from 3.16 mm to 2.24 mm, which may be caused by the increased utilization of wind energy for the rotation of the CBF. So, enlarging the transition part moment of inertia can also reduce the vibration of the structure.

Figure 17c shows the influence of the transition part mass center height on the vibration properties. It can be seen that the displacement presents the "V"-type with the elevation of the mass center height, and the minimum value 3.16 mm appears when the mass center height is 15 m. According to the analysis, the mass center height deviation from the mudline produces an additional moment of inertia $m_f h_f^2$; when it is equal to the original moment of inertia I_f, the displacement is the minimum, so the deviation is $\sqrt{I_f/m_f} = 14.48$ m, which is consistent with the figure. Therefore, it is better for the transition part mass center height to be designed near the deviation $\sqrt{I_f/m_f}$ to reduce the vibration.

6. Vibration Properties under Different Operation Loading Conditions

Also, the load RMS value was set to 10 kN. Figure 18 shows the tower-top displacements under the 1P/wind/3P load conditions of the theoretical model. It can be seen that the 1P/3P displacements are positively and negatively correlated with rotation frequency. When rotation frequency nears 0.1 Hz, the 3P frequency is close to 0.3 Hz (the natural frequency of the model), so 3P resonance [33] occurs. The 3P displacement is obviously higher than 1P and wind displacements. Therefore, close scrutiny is required when the 3P frequency is close to the natural frequency of the structure.

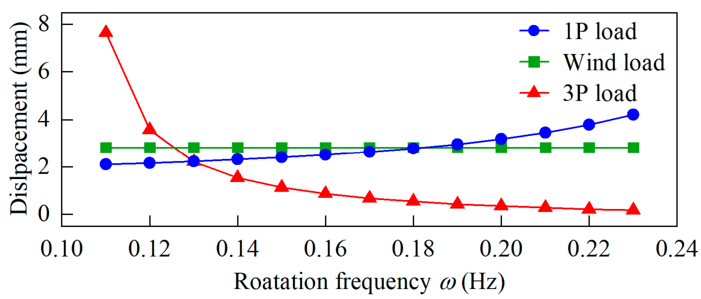

Figure 18. The displacements under different load conditions.

For the CBF structure mentioned in Section 2, the main frequencies of all 100 s data were extracted using the spectral analysis method and combined with the corresponding operation status, The distribution of the main frequency with rotation speed is presented in Figure 19.

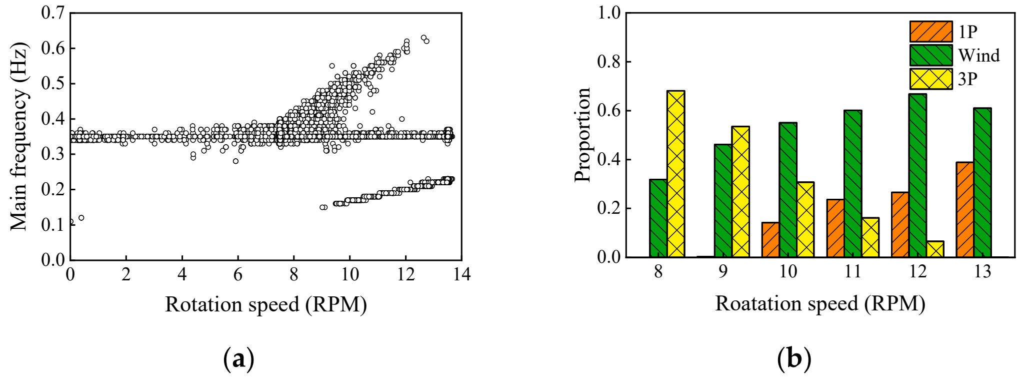

Figure 19. The distribution of the main frequency with rotation speed: (**a**) scatter; (**b**) histogram.

As shown in Figure 19a, the main frequency is concentrated in the first-order natural frequency of the wind turbine if rotation speed is less than 7.5 RPM. When rotation speed is higher than 7.5 RPM, the 1P/3P and natural frequencies are all reflected in the main frequency. The 3P frequency aggregates at the rotation interval near 7.5 RPM, which results from the 3P resonance caused by the 3P frequency 0.375 Hz approaching the natural frequency 0.35 Hz of the structure.

The occurrence frequencies of the main frequencies were recorded according to the speed range, and their proportion was calculated and plotted as shown in Figure 19b. It can be seen that the proportion of the 1P frequency increases, and the 3P proportion decreases gradually with respect to the increase in rotational speed. The natural frequency increases first and then decreases with the rotational speed. The 3P frequency is the most prominent main frequency at rotation intervals of less than 9 RPM, indicating that the 3P load has an important influence on this structure. Furthermore, the 1P load is less remarkable compared with 3P and wind loads. Dong XF et al. [35] tested the first full-scale CBF model and found that the 3P load has nearly no effect on the structure, which is quite different from the conclusion in this article. Therefore, the 3P load should not be ignored; it must be taken into account, lest excessive vibration or damage occurs.

7. Conclusions

A CBF prototype and monitoring system is introduced. By simplifying the CBF and whole wind turbine structure, a theoretical model was established and verified, the influence of the transition part parameters on the dynamic characteristics of the structure was studied and the vibration responses of operation loads were compared. The main conclusions are as follows:

(1) The transition part of the CBF can be regarded as a rigid body. Based on this simplification, the theoretical model of the CBF structure is accurate and reliable, and the errors of the displacement RMS and maximum values compared to the FEM results are 3.78% to 5.03%.

(2) The transition part mass mainly has a negative effect on the second-order natural frequency of the CBF structure, and the transition part moment of inertia only causes the third-order frequency reduction, while the mass center height has a slight influence on the natural frequencies.

(3) The transition part mass and moment of inertia mainly affect the horizontal and rotational stiffness of the CBF structure, respectively, with linear positive trends. In contrast, the influence of mass center height on the two stiffness of the foundation is consistent but limited.

(4) Enlarging both the transition part mass and moment of inertia can reduce the vibration of the CBF structure. The mass center shows a "V"-type trend for the vibration response, and the extreme value appears at the height of $\sqrt{I_f/m_f}$.

(5) From the theoretical analysis and the in situ measurement results, the 3P load has a great influence on the wind turbine if the 3P frequency is close to the natural frequency, and it should not be ignored.

With this work, the influence of transition part parameters on the CBF structure is clear and helpful for CBF design, and new knowledge on the vibration response difference between operation loads can guide the operation strategy optimization for wind turbines to reduce structural vibration.

Author Contributions: Conceptualization, J.L.; methodology, X.D. and H.Z.; validation, X.D. and J.L.; formal analysis, H.Z.; investigation, J.L., X.D. and H.Z.; resources, J.L.; data curation, X.D. and H.Z.; writing—original draft preparation, H.Z.; writing—review and editing, X.D.; visualization, H.Z.; supervision, X.D.; project administration, J.L.; funding acquisition, J.L. All authors have read and agreed to the published version of the manuscript.

Funding: This research was funded by the National Natural Science Foundation of China, grant number U21A20164.

Institutional Review Board Statement: Not applicable.

Informed Consent Statement: Not applicable.

Data Availability Statement: Data are contained within the article.

Conflicts of Interest: The authors declare no conflicts of interest.

References

1. Global Wind Report. 2023. Available online: https://gwec.net/globalwindreport2023/ (accessed on 27 March 2023).
2. Zhou, L.; Li, Y.; Liu, F.S.; Jiang, Z.Q.; Yu, Q.X.; Liu, L.J. Investigation of dynamic characteristics of a monopile wind turbine based on sea test. *Ocean Eng.* **2019**, *189*, 106308. [CrossRef]
3. Tu, Z.S.; Zhang, C.L.; Liu, H.Q.; Zhu, R.H. Hydrodynamic analysis of a multi-pile-supported offshore wind turbine integrated with an aquaculture cage. *J. Mar. Sci. Eng.* **2023**, *11*, 1830. [CrossRef]
4. Ku, C.Y.; Chien, L.K. Modeling of load bearing characteristics of jacket foundation piles for offshore wind turbines in Taiwan. *Energies* **2016**, *9*, 625. [CrossRef]
5. Oha, K.Y.; Namb, W.; Ryuc, M.S.; Kimc, J.Y.; Epureanu, B.I. A review of foundations of offshore wind energy convertors: Current status and future perspectives. *Renew. Sust. Energ. Rev.* **2018**, *88*, 16–36. [CrossRef]
6. Kapitanov, L.R.; Duroska, P.; Garcia, C.A.; Puigvert, M.M.; Ibsen, L.B.; Vandatirad, M.J. Literature review on cyclic lateral loading effects of mono-bucket foundations. In Proceedings of the 6th International Conference on Structural Engineering, Mechanics and Computation (SEMC), Cape Town, South Africa, 5–7 September 2016.
7. Penner, N.; Griessmann, T.; Rolfes, R. Monitoring of suction bucket jackets for offshore wind turbines: Dynamic load bearing behaviour and modelling. *Mar. Struct.* **2020**, *72*, 102745. [CrossRef]
8. Lian, J.J.; Sun, L.Q.; Zhang, J.F.; Wang, H.J. Bearing capacity and technical advantages of composite bucket foundation of offshore wind turbines. *Trans. Tianjin Univ.* **2011**, *17*, 132–137. [CrossRef]
9. Houlsby, G.T.; Kelly, R.B.; Huxtable, J. Field trials of suction caissons in clay for offshore wind turbine foundations. *Geotechnique* **2005**, *55*, 287–296. [CrossRef]
10. Houlsby, G.T.; Kelly, R.B.; Huxtable, J. Field trials of suction caissons in sand for offshore wind turbine foundations. *Geotechnique* **2006**, *56*, 3–10. [CrossRef]
11. Nielsen, S.D.; Ibsen, L.B.; Nielsen, S.A. Performance of a mono bucket foundation—A case study at Dogger Bank. *Int. J. Offshore Polar* **2017**, *27*, 326–332. [CrossRef]
12. Wang, B.; Qin, T.Q.; Yuan, C.F.; Li, L.; Yuan, M.H.; Li, Y. Analysis of bearing performance of monopile and single suction bucket foundation for offshore wind power under horizontal load. *Geofluids* **2022**, *2022*, 4163240. [CrossRef]
13. Zhang, P.Y.; Li, J.Y.; Le, C.H.; Ding, H.Y. Seismic responses of two bucket foundations for offshore wind turbines based on shaking table tests. *Renew. Energ.* **2022**, *187*, 1100–1117. [CrossRef]
14. Liu, X.X.; Chen, X.G.; Liu, J.Z.; Yu, T.S.; Sun, B.S. Scour effects on cyclic response of bucket foundations under waves and currents. *J. Coastal Res.* **2021**, *37*, 670–682. [CrossRef]
15. Song, H.Y.; Yu, T.S.; Yu, D.Y.; Zhao, Z.S. Hydrodynamic behavior of composite bucket foundation with random waves. *Ocean Eng.* **2023**, *281*, 114774. [CrossRef]
16. Liu, G.W.; Zhang, Q.H.; Zhang, J.F. Wave forces on the composite bucket foundation of offshore wind turbines. *Prog. Ind. Civil Eng. II* **2013**, *405–408*, 1420–1426. [CrossRef]
17. Ding, H.Y.; Pan, C.; Zhang, P.Y.; Wang, L.; Xu, Y.L. Shaking table tests and seismic response of three-bucket jacket foundations for offshore wind turbines. *J. Ocean Univ. China* **2022**, *21*, 719–736. [CrossRef]

18. Ding, H.Y.; Li, J.Y.; Le, C.H.; Pan, C.; Zhang, P.Y. Shaking table tests of four-bucket jacket foundation for offshore wind turbines. *China Ocean Eng.* **2022**, *36*, 849–858. [CrossRef]
19. Jalbi, S.; Nikitas, G.; Bhattacharya, S.; Alexander, N. Dynamic design considerations for offshore wind turbine jackets supported on multiple foundations. *Mar. Struc.* **2019**, *67*, 102631. [CrossRef]
20. Ding, H.Y.; Feng, Z.T.; Zhang, P.Y.; Le, C.H.; Guo, Y.H. Floating Performance of a Composite Bucket Foundation with an Offshore Wind Tower during Transportation. *Energies* **2020**, *13*, 882. [CrossRef]
21. Lian, J.J.; Zhou, H.; Dong, X.F. Study on structural vibration behavior and vibration reduction of bucket foundation wind turbines. *J. Hydroe. Eng.* **2022**, *41*, 1–9. (In Chinese)
22. Kraemer, P.; Friedmann, H. Vibration-based structural health monitoring for offshore wind turbines—Experimental validation of stochastic subspace algorithms. *Wind Struct.* **2015**, *21*, 693–707. [CrossRef]
23. Sun, G.D.; Liu, R.; Li, Q.X.; Huang, G.Y.; Zhou, Z.B.; Zhang, C. Research on the Critical Buckling Pressure of Bucket Foundations with Inner Compartments for Offshore Wind Turbines. *Ocean Univ. China* **2023**, *22*, 419–428. [CrossRef]
24. Sun, C.; Jahangiri, V. Bi-directional vibration control of offshore wind turbines using a 3D pendulum tuned mass damper. *Mech. Syst. Signal Pr.* **2018**, *105*, 338–360. [CrossRef]
25. Clough, R.W.; Penzien, J. *Dynamics of Structures*, 3rd ed.; Computers & Structures, Inc.: Walnut Creek, CA, USA, 2003.
26. Brasil, R.M.L.R.; Feitosa, L.C.S.; Balthazar, J.M. A nonlinear and non-ideal wind generator supporting structure. *Appl. Mech. Mater.* **2006**, *5–6*, 433–442. [CrossRef]
27. Bao, W.B.; Bai, Q.; Lu, H.Y. *Fundamentals and MATLAB Applications of Vibration Mechanics*; Tsinghua University Press: Beijing, China, 2015.
28. Carswell, W.; Johansson, J.; Lovholt, F.; Arwade, S.R.; Madshus, C.; DeGroot, D.J.; Myers, A.T. Foundation damping and the dynamics of offshore wind turbine monopiles. *Renew. Energ.* **2015**, *80*, 724–736. [CrossRef]
29. Lei, Y.J.; Zhang, S.W. *Toolbox and Application of Genetic Algorithm in MATLAB*; Xidian University Press: Xi'an, China, 2014.
30. Ogunjuyigbe, A.S.O.; Ayodele, T.R.; Bamgboje, O.D. Optimal placement of wind turbines within a wind farm considering multi-directional wind speed using two-stage genetic algorithm. *Front. Energy* **2021**, *15*, 240–255. [CrossRef]
31. Poudel, P.; Kumar, R.; Narain, V.; Jain, S.C. Power optimization of a wind turbine using genetic algorithm. In Proceedings of the 4th International and 19th National Biennial Conferences on Machines and Mechanisms (iNaCoMM), Suran, India, 5–7 December 2019.
32. Tian, J.M.; Tan, X. The Optimization Design of Wind Turbine Gearbox Based on Improved Genetic Algorithm and Feasibility Analysis. In Proceedings of the 4th International Conference on Advances in Materials and Manufacturing (ICAMMP 2013), Kunming, China, 18–19 December 2013.
33. Lian, J.J.; Zhou, H.; Dong, X.F. A theoretical approach for resonance analysis of wind turbines under 1P/3P loads. *Energies* **2022**, *15*, 5787. [CrossRef]
34. *DNV-OS-J101*; Design of Offshore Wind Turbine Structures. Det Norske Veritas: Oslo, Norway, 2011.
35. Dong, X.F.; Lian, J.J.; Wang, H.J. Vibration source features of offshore wind power structures under operational conditions. *J. Vib. Shock* **2017**, *36*, 21–28. [CrossRef]